A study of mechanical properties and microstructure in friction stir welded thin sheet aluminium alloys

E. Cerri, P. Leo, X. Wang, D. Embury

Friction stir welding of very thin aluminium sheets represents a potential goal for aircraft and automotive industries due to the advantages of using this new technological process. In the present work, the microstructural evolution and mechanical behaviour of 6082T6-2024T3 thin friction stir welded joints were investigated. Uniaxial tensile testing at room temperature, 170°, 200° and 230°C were performed in order to determine the extent to which these ultra thin joints can be used and deformed. The tensile stress-strain curves showed a decrease of the flow stress with increasing temperature and decreasing strain rate.
At 230°C recovery mechanisms (dislocation reorganization inside the deformed grains) initiated but the temperature was not enough high to produce a homogeneous subgrain structure.

Keywords:
mechanical properties, fsw thin joints, aluminium alloys

INTRODUCTION

Friction stir welding (FSW) is a solid state joining method particularly suited for aluminium alloys, which are often difficult to fusion weld without hot cracking, porosity or distortion. During welding, the material is frictionally heated to a temperature, at which it becomes extremely plastic. The heat of friction and plastic flow arising from the rotating tool produce significant microstructural changes, which lead to local variations in the mechanical properties of the weld [1-5]. FSW is being targeted by the industry for structurally demanding applications to provide high-performance benefits [6]. The weld zone consists of a stir zone, a thermomechanically affected zone (TMAZ) and a heat affected zone (HAZ). The grain size in the stir zone is very fine and equiaxed resulting in a higher mechanical strength and ductility [7-13].
In FSW the work piece does not reach the melting point and the mechanical properties such as ductility and strength of the welded zone are much higher compared to the traditional welding techniques [14-17].
Actually, this is a core demand of aircraft and car industries to substitute the traditional joining technologies with low cost and high efficiency ones such as FSW in the future advanced design. Recent literature reports examples of FSW of dissimilar aluminium alloys [18-20], as well as aluminium-steel [21,22], aluminium-magnesium [23] and aluminium-silver [24].
Friction Stir Welding (FSW) is well established for making butt joints in aluminium alloys in material thicknesses from 1.3 to 15mm and plates up to 50 mm thick have been welded experimentally. In contrast, the welding of thin sheets in thicknesses of 1mm and below has not been systematically explored. However, production welding of thin sheets, especially involving lap joints, could provide significant cost savings and improved weld quality and new design opportunities for numerous industries, such as aerospace, automotive and electronic packaging.
The aim of this work is to study the deformation behaviour at warm and room temperatures of very thin FSW sheets of aluminium alloys, combined in similar and dissimilar butt joints. The choice to investigate tensile properties at warm temperature of straining is related to the feasibility of drawing such thin welded joints. The joints were characterized by macrographic and micrographic examinations, microhardness, tensile tests, TEM and X-Ray diffractometry to follow the microstructure evolution and mechanical properties variations.

E. Cerri, P. Leo
Dept. of Innovation Engineering, University of Salento,
via per Arnesano, 73100 Lecce - Italy
X. Wang, D. Embury
Dept. of Materials Science and Engineering, Mc-Master University,
Hamilton, Ontario, L8S 1XS - Canada

EXPERIMENTAL DETAILS

Two materials form the basis of this study: 2024-T3 and 6082-T6 aluminium rolled sheets of 0.8 mm thick. These sheets have been friction stir welded by a cylindrical non-threaded probe of 1.7 mm in diameter and 0.6 mm in height (the tool shoulder was 6 mm in diameter). The welding tool was made of 56NiCrMoV7 tool steel. Base materials (Table 1 for chemical composition) were welded parallel to the rolling directions with a weld and rotational speed of 762 mm/min, 2085 rpm respectively. The weld parameters were optimised taking into account the mechanical properties of the softer alloy. The grain size and microstructural features have been observed by light microscopy on a Nikon Epiphot equipped with an image analyzer. For metallographic observations, samples were mechanically ground and polished up to 1 μm diamond paste. Chemical etching was performed by Keller's reagent and if anodized, a solution of 5% HBF_4 in Methanol was used to reveal grains by polarized light. Microhardness profiles were measured in the cross section of the thin welded joints by applying a load of 500 g for 15s. Specimens for tensile tests,

	Cu	Mg	Mn	Fe	Si	Zn	Cr	Ti	Al
6082T6	0.08	0.78	0.48	0.39	0.95	0.04	0.03	0.05	rem
2024T3	4.67	1.34	0.63	0.25	0.15	0.02	0.01	0.06	rem

TAB. 1 ***Chemical composition (% in weight) of the base materials.***

Chemical composition (% in weight) of the base materials.

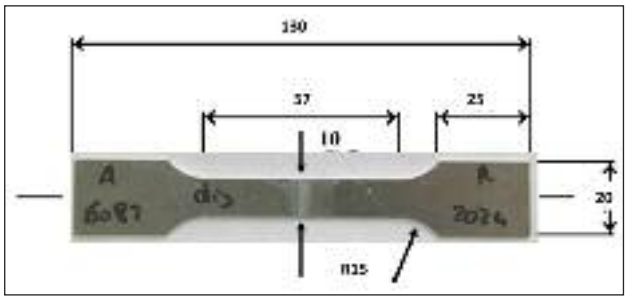

FIG. 1 ***Scheme of tensile samples according to UNI EN 1002/5.***

Schema del campione di trazione second UNI EN 1002/5.

with a gauge length of 57 mm, a width of 10 mm and thickness of 0.8 mm according to UNI EN 1002/5, were machined from the FSW sheets in order to have the loading axis normal to the welding direction (Fig. 1). An extensometer was employed to measure the elongation and it was positioned such that junction line corresponded to the middle point of the initial gage length. The tensile tests were performed at 170°, 200° and 230°C and nominal strain rates of 10^{-3}, 10^{-4}, $5x10^{-5}$ s^{-1} to study the warm temperature deformation behaviour of the similar and dissimilar joints. A set of tests was run at room temperature at a nominal initial strain rate of 10^{-4} s^{-1}. Three tests were run at least for each experimental condition to assure measurements accuracy. All the tensile tests were performed by an Instron 4485 equipped with a cylindrical furnace for warm temperature deformation tests.

TEM samples were prepared from the base materials (at least 30 mm far away from the stir zone) and from the stir zone on the rolling plane, due to the very thin cross section. A PHILIPS CM12 TEM was used to characterize the microstructure of samples. After mechanical grinding down to approximately a thickness of 100 μm, 3 mm diameter discs were punched followed by twin-jet electropolishing in a 10 vol% perchloric acid in methanol solution, at -35°C and 15V.

X-rays diffraction was performed on several strained samples to sudy precipitate evolution in the strained regions. Measurements were carried out with a Cu radiation using a step size of 0,05° and step time of 20 s.

RESULTS AND DISCUSSION

Metallography of the welds

Optical micrographs of the thin friction stir welded joint are illustrated in Figs. 2. The weld exhibits distinct regions as shown in Fig. 2: the Base Material (or parent material), HAZ, TMAZ and stirred zone for the 6082T6 on the left side and the stirred zone, TMAZ, HAZ and BM for the 2024T3 on the right. The stirred zone is the region where the highest strain is experienced and where recrystallization occurred. Its microstructure is the results of the mechanical action of the tool probe that generates a recrystallization process. By moving towards the BM, no recrystallization was observed in TMAZ and in HAZ.

The images also show that these thin joints are of good quality because no defects or porosity were detected demonstrating the

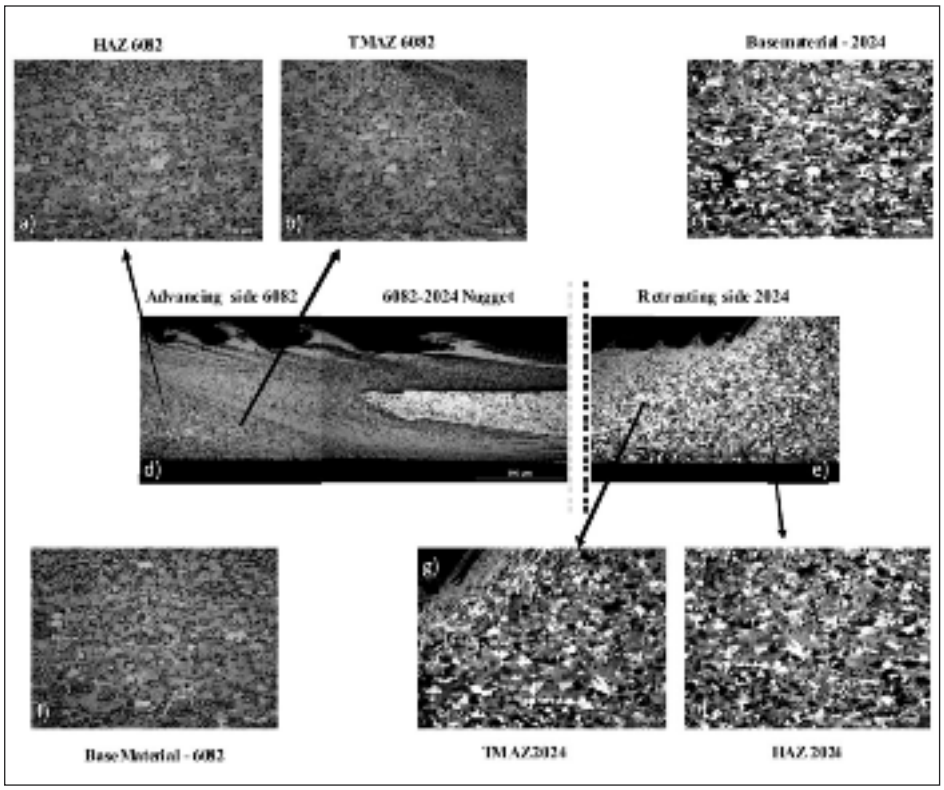

FIG. 2

Microstructure of the 6082T6-2024T3 FSW joint with the advancing side (6082T6) presented on the left side of the picture: (a) Heat Affected Zone (HAZ) of the 6082T6, (b) Thermo mechanically Affected Zone (TMAZ) of the 6082T6; (c) Base material of the 20204T3; (d) low magnification picture of the HAZ 2024T3; (e) retreating side; (f) Base material of the 6082T6; (g) TMAZ and (h) HAZ of the 2024T3.

Microstruttura del giunto 6082T6-2024T3 con l'advancing side sul lato sinistro della figura: : (a) Zona Termicamente Alterata (HAZ) of the 6082T6, (b) Zona termomeccanicamente alterata (TMAZ) della 6082T6; (c) materiale base della 2024T3; (d) foto a bassi ingrandimenti di HAZ 2024T3; (e) retreating side; (f) materiale base della 6082T6; (g) TMAZ e (h) HAZ della 2024T3.

complete weldability of these two alloys at the solid state. The BM, the HAZ and the TMAZ are also clearly distinguishable.

Microhardness profiles

The variation in hardness with distance from the centre of the stir zone has been measured across the original weld. Fig. 3 shows the hardness profiles, starting from the BM to the centre of the weld, in the advancing and retreating directions. The profile differs for the retreating and advancing side, according to thermal treatments and microstructure of 2024T3 and 6082T6. In the stir zone of the 2024T3 side, the hardness is in the range of 130-140 HV. The fluctuations are due to onion ring structure present in the nugget and to associated precipitate distribution which influences the microhardness measurements from point to point [26,27]. The microhardness is slightly high in the nugget with respect to the TMAZ and HAZ because of the finer grain size present in the nugget. The HV profile for the 6082T6 Base Materials shows values of 105-110 HV (less scattered values respect to the 2024T3 side) but a drop of almost 30 HV in the stir zone is detected. The starting condition of the 6082 sheet is T6 and during the FSW process, the temperature in the nugget may even reach 350-450°C [10, 28], depending on experimental conditions. From a microstructure point of view, this can lead to an evolution of precipitates towards coarsening or partial dissolution and results in a decrease in hardness, even if the grains are refined by the process. In Fig. 3, the hardness profiles, taken in the same sample but at different distances from the top and bottom surfaces, are compared with the profile measured in the centre of the sample. It results a difference of also 60 HV in a distance of 1mm around the nugget centre. In fact, near the top of surface, due to the effect of the shoulder the heat generated is higher than near the base of the pin. This could affect hardness. However, depending upon the geometry of the pin, the plastic deformation around the pin could be severe which in turn could vary the grain size and possibly affect hardness as shown in Fig. 3. In this paper, in order to have a reference in hardness measurements, the authors decided to take HV measures at mid height of every joint.

TEM analysis of original joints

The microstructure of the BM in the 2024T3 is illustrated in Fig. 4. A high density large rod shaped particles (Fig. 4a) containing Al, Mn, and Cu (see EDX spectrum Fig. 4d) (probably $Al_{20}Mn_3Cu_3$) are visible. It is believed that the rod shaped particles containing Mn and Cu are formed during solidification. They are homogeneously distributed in the matrix and aligned along a preferential direction (rolling direction) in different grains. A mean radius of 0.05 μm and an aspect ratio of 2 ~ 3 are estimated. There was no evidence for the existence of fine particles. High density dislocations were observed particularly around the particles (Fig. 4c).

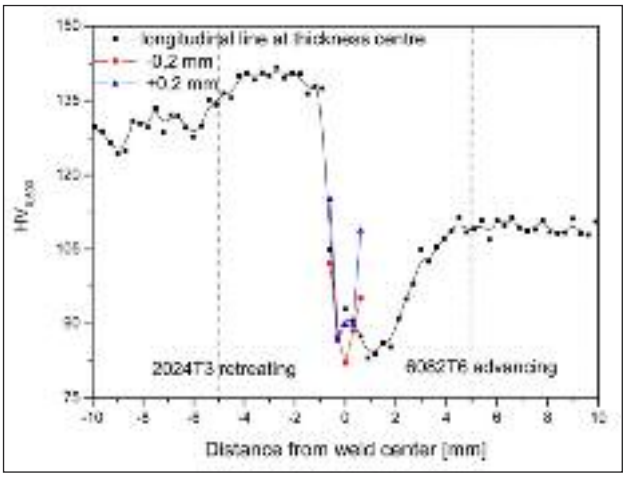

FIG. 3 ***Microhardness profiles of the thin FSW joint measured at the middle of the cross section of the dissimilar joint, at 0.2 mm from the top and at 0.2mm from the bottom.***

Profili di microdurezza del giunto misurati al centro dello spessore, a 0,2mm dalla superficie superiore (top) e a 0,2 mm dalla sup. inf. del giunto.

The microstructure of the BM in the 6082T6 is seen in Fig. 5. Large spherical insoluble particles (Fig. 5a) of Al(Fe,Mn,Cu,Cr)Si type (see EDX spectrum in Fig. 5b) are homogeneously distributed in the matrix. These particles have an average diameter of approximately 0.2 μm. It is believed that the particles are dispersoids, which formed during solidification and that the solution treatment and aging processes have no substantial effect on them. In addition, the BM contained a high density of homogeneously distributed needle shaped β" precipitates, giving characteristic streaks in diffraction pattern at high magnification because of very their fine dimensions (Fig. 5c).

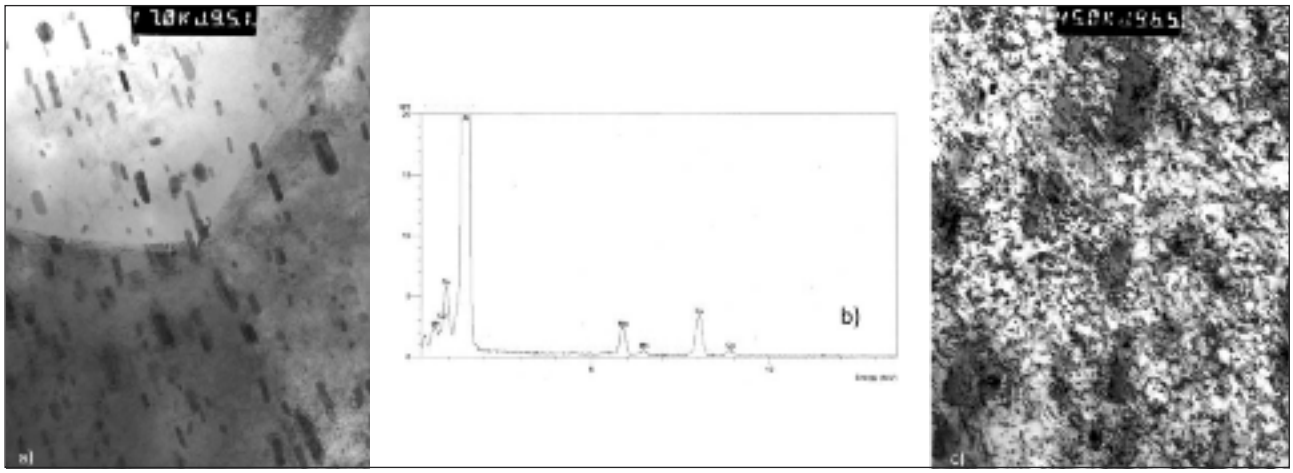

FIG. 4 ***Microstructure in the 2024T3 BM. TEM micrographs showing (a) AlMnCu type particles, b) EDX spectrum of particles in (a), (c) dislocation density.***

Microstruttura del materiale base 2024T3. Micrografia TEM con (a) particelle tipo AlMnCu, b) spettro EDX delle particelle in (a), (c) densità delle dislocazioni.

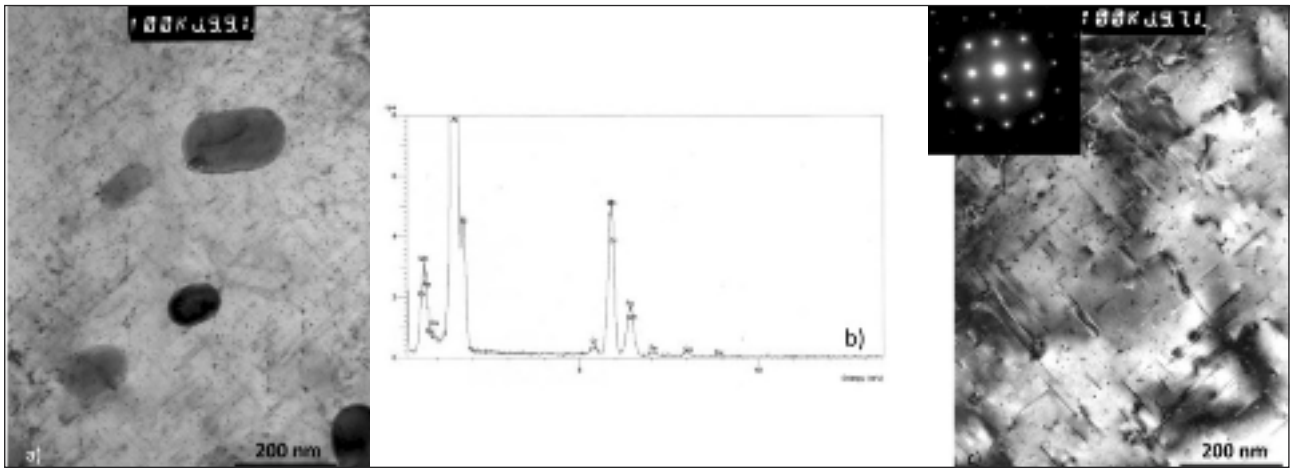

FIG. 5 ***Base Material in 6082T6. TEM micrographs showing a) large insoluble particles with (b) EDX spectrum, c) homogeneously distributed β" precipitates in Bright Field and d) in Dark Field. e) X-Rays diffractometry of the three zones of the dissimilar joint.***

Materiale base nella 6082T6. Micrografia TEM con (a) particelle insolubili, (b) spettro EDX, (c) precipitati β" omogeneamente distribuiti (DF) e (d) BF. (e) diffrattogramma X delle tre parti del giunto 6082T6-2024T3.

The detailed precipitates size and distribution were revealed by dark field image at high magnification (fig. 5d), which showed that besides majority of β" precipitates, also a small amount of precursor of β (GP zone of the AlMgSi system) phase can be found. There was no evidence for existence of precipitate free zones (PFZ).

X-Rays investigations have been performed on BM and in the nugget zones to study particle evolution. Fig. 5e shows the comparison of the two base materials with the stirred zone in the dissimilar joint. X-Rays analysis confirms the presence of Al-MnCu and AlFe(Si,Cu) type particles in the 2024T3 BM and of AlFeSi type intermetallics in the 6082T6 BM. The nugget zone shows no significant presence of intermetallics that can be revealed by X-Rays diffractometry in the same experimental conditions used. Moreover, the Aluminium peaks of the BMs and of the stir zone perfectly overlap. This means that the lattice constants of Al alloys are not changed in the stir zone by the FSW process and no additional residual stresses are present in the nugget respect to the Base Materials [29].

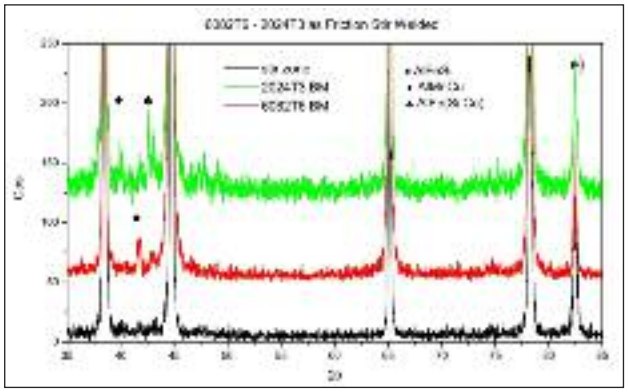

FIG. 6 ***Base Material in 6082T6. TEM micrographs showing a) large insoluble particles with (b) EDX spectrum, c) homogeneously distributed β" precipitates in Bright Field and d) in Dark Field. e) X-Rays diffractometry of the three zones of the dissimilar joint.***

Materiale base nella 6082T6. Micrografia TEM con (a) particelle insolubili, (b) spettro EDX, (c) precipitati β" omogeneamente distribuiti (DF) e (d) BF. (e) diffrattogramma X delle tre parti del giunto 6082T6-2024T3.

Tensile behaviour

The evaluation of tensile properties at room temperature of the FSW joints is reported in Fig. 6a. The stress-strain curves of 6082T6-2024T3 joint are compared with 2024T3-2024T3 and 6082T6-6082T6 joint curves. The elastic part of the stress-strain curves overlap showing a good correspondence in elastic modulus even for the dissimilar joint (≈ $25x10^3$ MPa). The plastic behaviour is illustrated by strain hardening occurring in all the joints. The dissimilar joint shows a median strength of 260 MPa but has the lower ductility.

Several tensile tests have been performed at temperatures in the range of 170°- 230°C to study the mechanical response of the thin joints at warm temperatures of deformation. A complete evaluation of tensile tests results at all temperatures and strain rates investigated is illustrated in Fig. 6b, showing the values of the Yield Strength YS, Ultimate Tensile Strength UTS and true strain ε. The thin dissimilar joint presents values of UTS and YS quite similar because of fracture occurred at a percentage of elongation of 2 or 3%. The trend for the UTS and YS is to slightly decrease with decreasing strain rate and increasing temperature. In general the ductility is rather poor for the dissimilar joint even at warm temperature of deformation.

Microhardness measurements have also been performed on the joint samples after deformation at room temperature (Fig. 7) in order to evaluate the strain hardening distribution. The strain hardening contributes to hardness curves of the investigated joints in different ways. In the 6082T6 side, the strain hardening contribution to hardness measurements is visible in the nugget zone, where the hardness profile has a peak instead of being flat as in the original weld. The region of the weld was the softer one before deformation. In the 2024T3 side, the strain hardening slightly contributes to hardness with an increase of few points most of which in the HAZ and BM respect to the unstrained sample.

TEM analysis of FSW joints after tensile tests at 170°, 200° and 230°C

In order to investigate the deformed FSW joints by TEM, samples were cut from the stir zone and far from the welding region

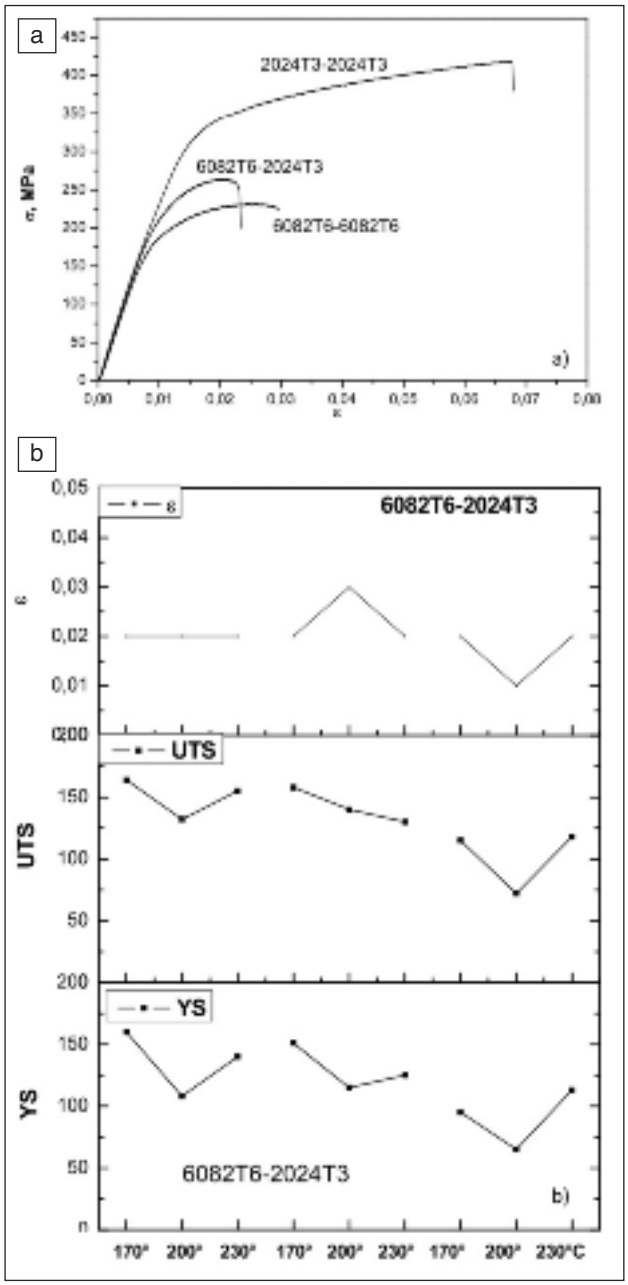

FIG. 7 ***Stress-strain curves (a) of dissimilar joints compared with similar joints and (b) tensile properties at warm temperature of deformation.***

Curve tensione-deformazione (a) del giunto dissimile e simili; (b) proprietà tensili a temperature di deformazione intermedie.

in the gauge part of fractured tensile tested samples that deformed at 230°C and strain rate of 10^{-5} s^{-1}. The examination of these samples is connected to the time duration of the tests (the longest - almost one hour) and to the highest temperature of deformation.

Fig. 8 shows the microstructure of the 2024T3 BM in the 6082T6-2024T3 joint after warm temperature straining. In the sample there are a high density of large rod shaped particles (Fig. 8a) formed during solidification with similar size as in the parent material (Fig. 4). They are homogeneously distributed and align along preferred directions. In addition, fine rod shaped S'(S) precipitates (Fig. 8b in BF and 8c in DF) formed due heating during tensile test. Dislocations are also homogeneously di-

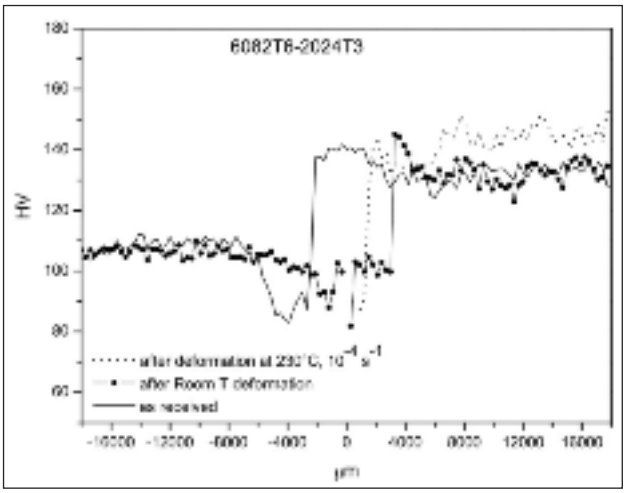

FIG. 8 ***Microhardness profiles of the FSW joint (as received) compared with joints after deformation at room temperature and at 230°C, 10^{-4} s^{-1}.***

Microdurezza del giunto come ricevuto e dopo deformazione a freddo e a 230°C, 10^{-4} s^{-1}.

stributed in the matrix and PFZs at grain boundaries have not been found.

TEM micrographs of the 6082T6 BM after warm temperature deformation (Fig. 9) show, in addition to near spherical insoluble particles (Fig. 9b) and needle-shaped β" present in the BM of the starting sample, a small amount of precursor of β or Q precipitates (Fig. 9a). Qualitatively, the size of precipitates is similar to those in the parent material. In this case a PFZ formed at grain boundaries and the dislocation density is low.

For the nugget (Fig. 10) TEM investigations illustrates very fine grains (Fig. 10a) and particles encountered in the two aluminium alloys. Some of these grains contain a high number of dislocations that are still organizing in cell structures but cell structure formation appears inhibited by particle interactions.

The mode of fracture of tensile tested sample is shown in Fig. 11. The rupture occurred in the middle of the stir zone after a slight necking is formed. This behaviour occurred in all the investigated samples and suggested that the stir zone has a lower plastic deformation capability than the rest of the sample. For more accurate examinations of fracture surfaces, tensile samples were cut close to the fracture surface, in the direction perpendicular to the tensile axis, for scanning electron microscopy observations. Figs. 11a and 11c are fracture surfaces of the dissimilar joint tensile tested at 230°C, 10^{-4} s^{-1}, while the right column shows fracture surfaces from samples deformed at 10^{-3} s^{-1}. SEM investigations demonstrated a ductile mode of fracture in all the conditions. In these samples, moreover, layers of different thickness (Fig. 11a and 11b) are visible due to the presence of the two aluminum alloys in the stir zone, together with fine dimples.

DISCUSSION

The mechanism occurring during warm deformation of the 6082T6-2024T3 joints can be explained with regards to dynamic precipitation and substructure modification in the nugget during straining. In the FSW joint, it is supposed that the nugget and closest zones have experienced peak temperatures between 200° and 350°C [30] during the joining process, in a very short time, due to the thin thickness of the sheets. Particles of S'(S) and GPB (Guinier-Preston-Bagaryatsky zones) [30-32] type should be present in the nugget after joining, together with di-

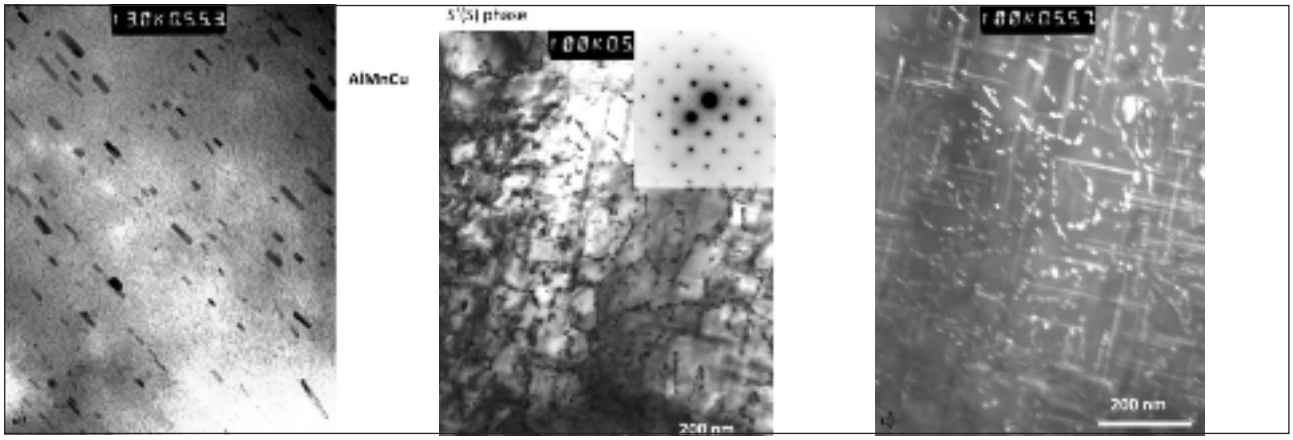

FIG. 9 ***TEM micrographs of the BM in the 2024T3 after tensile test at 230 °C and 10^{-5} s^{-1}. Rod shaped AlMnCu particles (a) and fine S'(S) particles formed during tensile test exposure in BF (b) and in DF (c).***

Micrografie TEM del materiale base 2024T3 dopo trazione a 230 °C e 10^{-5} s^{-1}. Particelle di AlMnCu (a) e precipitate fini di S'(S) formati durante il test a caldo in BF (b) e DF (c).

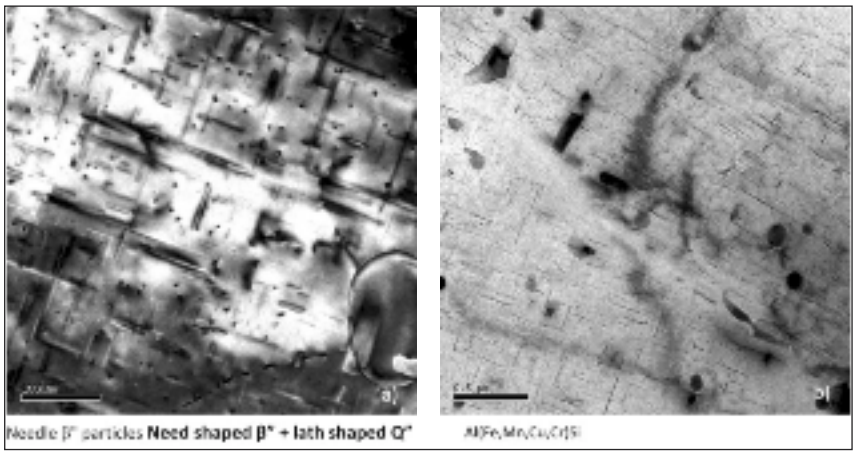

FIG. 10
TEM micrographs of the BM in the 6082T6 after tensile test at 230 °C and 10^{-5} s^{-1}. High magnification pictures showing (a) needle β" particles and lath shaped Q" and (b) near sphere insoluble Al(Fe,Mn,Cu,Cr)Si particles.

Micrografie TEM del materiale base 6082T6 dopo trazione a 230 °C e 10^{-5} s^{-1}. Foto ad elevato ingrandimento con (a) particelle β" e Q" e (b) particelle quasi insolubili del tipo Al(Fe,Mn,Cu,Cr)Si.

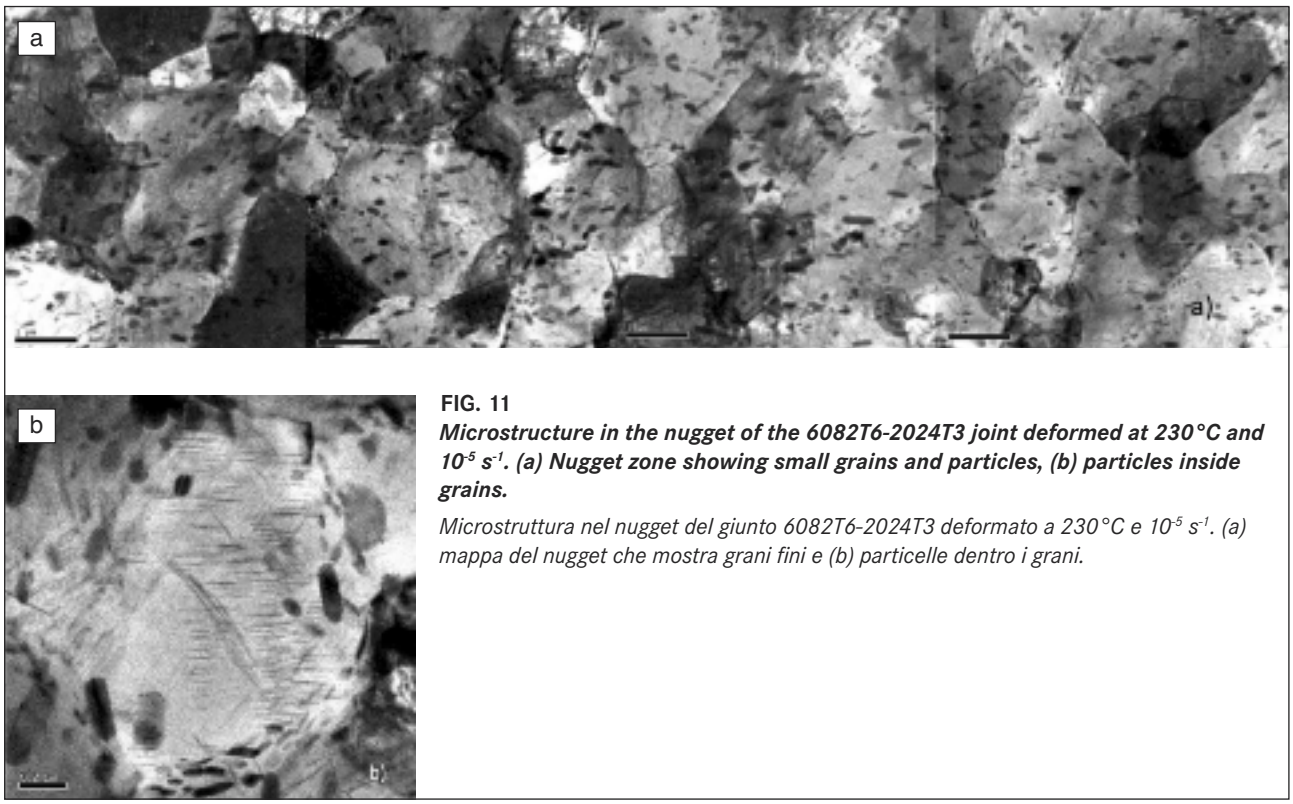

FIG. 11
Microstructure in the nugget of the 6082T6-2024T3 joint deformed at 230 °C and 10^{-5} s^{-1}. (a) Nugget zone showing small grains and particles, (b) particles inside grains.

Microstruttura nel nugget del giunto 6082T6-2024T3 deformato a 230 °C e 10^{-5} s^{-1}. (a) mappa del nugget che mostra grani fini e (b) particelle dentro i grani.

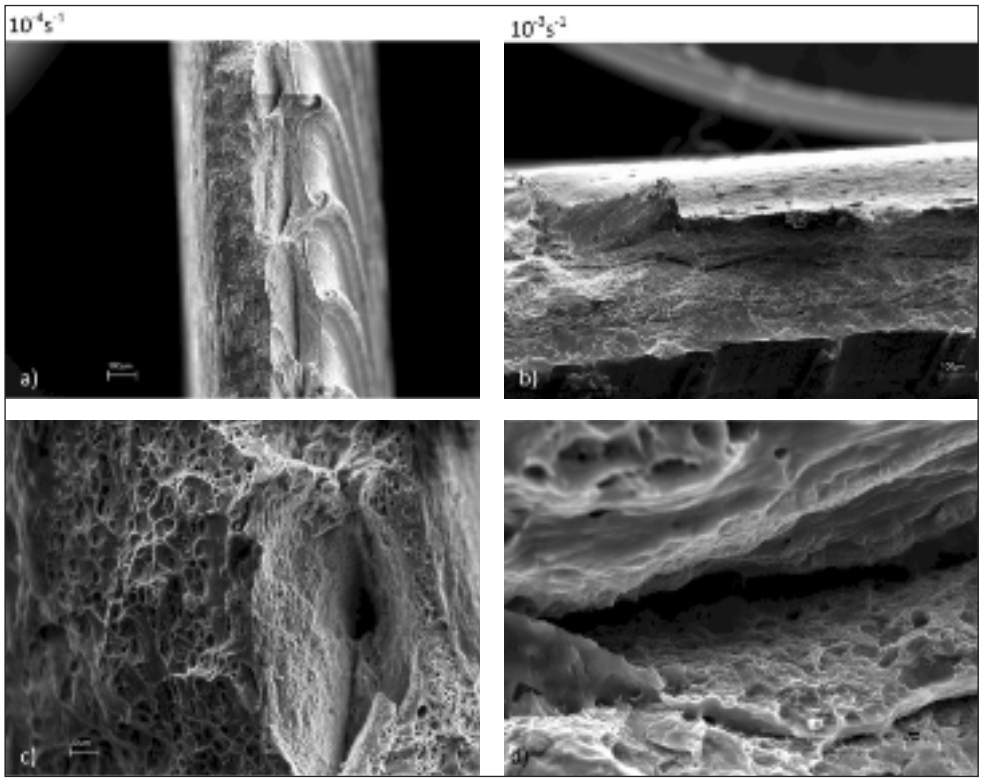

FIG. 12
Mode of fracture of the 6082T6-2024T3 FSW joints, tensile tested at 230°C and at 10^{-4} s^{-1} (left column) and at 10^{-3} s^{-1} (right column). (a) and (b) low magnification picture showing the fracture occurring in the middle of the stir zone; (c) and (d) high magnification micrographs showing dimples.

Tipologia di frattura nei giunti 6082T6-2024T3 trazionati a 230°C e 10^{-4} s^{-1} (colonna di sinistra) e 10^{-3} s^{-1} (colonna di destra). (a) e (b) foto a basso ingrandimento della zona di frattura in mezzo al nugget; (c) e (d) microvuoti nelle zone di frattura.

spersoids of the AlMnCu type, already found in the 2024T3 BM. The aspect ratio of these large particles is modified due to thermomechanical process of joining. The warm temperature of deformation of these joints, i.e. at 230°C, induces modification of dislocation organization and interaction between dislocation and precipitates as a function of the imposed strain rates. The elongation becomes rather poor with decreasing strain rate at 230°C. TEM performed in these joints have shown the presence of S'(S) precipitates, coarse and fragmented AlMnCu particles, and dislocation homogeneously distributed. The reason of a decreasing ductility with decreasing strain rate may reflect a progressive decrease of strength due to strain localization. On the other hand, homogeneity of deformation has been kept at the lower strain rate, because the smaller precipitates had insufficient time to change (duration time almost 60s for tensile test performed at $10^{-3}s^{-1}$).

The deformation mechanism in the dissimilar joints is complex because the weld zone is the results of mixing the two alloys as seen in Fig. 10. The elongation to failure seems to be rather poor and the ductile fracture surfaces present very fine dimples but also voids of at least 50 μm in length (as measured by SEM) under the upper surface. The premature rupture of the dissimilar FSW joints may be caused by premature void formation during tensile tests under onion rings. According to the optical micrograph shown in Fig. 2, the bigger voids seen in Fig. 11c and 11d belong to the 6082T6 alloy. So it is the softer alloy (the 6082T6) that determines the mechanical behavior during tensile deformation of the dissimilar joints, in the range of investigated temperatures and strain rates. Concerning the microstructure of the dissimilar joints during deformation, TEM investigations have shown the presence of particles belonging to 6082T6 and 2024T3 alloy, depending on which zone was investigated in the nugget.

SUMMARY AND CONCLUSIONS

Very thin FSW joints in 6082T6-2024T3 aluminium alloys of 0,8 mm in thickness were subjected to a number of tensile tests at room and warm temperatures combining heating (typical aging temperatures) at the same time with plastic deformation. The aim of these experiments is to gain some understanding on mechanical properties and on the effect of plastic deformation on the microstructure of very thin aluminium alloy FSW joints. The microstructure evolution was studied by polarized light microscopy, TEM and X-Rays. The following conclusions were drawn from the results.

- the thin FSW joints showed the capability to undertake tensile stress at room temperature and at warm temperatures of deformation. The stress decreased with increasing temperature and decreasing strain rate. The ductility of the thin joints was in general rather poor and quite independent by temperature and strain rate. As the aim the tensile tests conducted at warm temperatures was to understand the capability of these thin joints to be deformed for technological process like drawing or similar operations, one can conclude that the warm temperature induces a decrease in the flow stress and this can be positive, but there is not an increase in ductility to permits strong deformation processes for these thin joints.
- TEM investigations performed on the parent materials and on the strained joints evidenced: a) in the 2024T3 BM the precipitation and growth of S' type phases that help the microstructure to have a higher strength than the 6082T6. No PFZ were observed at grain boundaries. b) In the 6082T6 BM, β'' precipitates were already present from the beginning because of the T6 state and during warm temperature deformation, they grow slightly lowering their contribution to the strength. Moreover, PFZ were observed in these joints. c) The warm deformation temperature of 230°C was enough to permit the dislocations to reorganize inside the deformed grains but not enough to have a homogeneous subgrains structure.
- Tensile specimen fractured in the middle of the stir zone after straining at room temperature or at warm temperature of deformation in a ductile mode. Anyway, even if the ductility was comparable in different specimens, the microvoid size, distribution and coalescence is variable from sample to sample, probably depending on the dominant void nucleation mechanism.

ACKNOWLEDGEMENTS
The authors would like to thank Ing. P.P. De Marco and Ms. Todisco for precious help in laboratory techniques. Supply of materials from Politecnico di Bari is gratefully acknowledged. Authors thank MIUR for fundings.

REFERENCES
[1] C.G. Rodes, M.W. Mahoney, W.H. Bingel, R.A. Spurling, C.C. Bampton, Scripta Mater. 36 (1997) 69-75.
[2] M.W. Mahoney, C.G. Rodes, J.G. Flintoff, R.A. Spurling, W.H. Bingel, Metall. Mater. Trans. A 29 (1998) 1955-1964.
[3] Y. Sato, H. Kokawa, M. Enomoto, S. Jogan, Metall. Mater. Trans. A 30 (1999) 2429-2437.
[4] K.V. Jata, Mater. Sci. Forum 331-337 (2000) 1701-1712.
[5] R. Braun, C. Dalle Donne, G. Staniek, Mat. -Wiss. u. Werkstofftech. 31 (2000) 1017-1026.
[6] W.M. Thomas, E.D. Nicholas, J.C. Needam, M.G. Murch, P. Templesmith, C.J. Dawes, GB Patent application 9125978.8 (1991); 9125978.8, December 1991 and US Patent No. 5460317, October 1995.
[7] I. Charit, R. S. Mishra, M. W. Mahoney, Scripta Mater. 47 (2002) 631-636
[8] H. G. Salem, A. P. Reynolds, J. S. Lyons, Scripta Mater. 46 (2002) 337-342.
[9] C.G. Rhodes, M.W. Mahoney, W.H. Bingel, M. Calabrese, Scripta Mater. 48 (2003) 1451-1455
[10] K.V. Jata, S.L. Semiatin, Scripta Mater. (2000) 43 (8) 743-749.
[11] W. D. Lockwood, B. Tomaz, A.P. Reynolds, Mater. Sci. and Eng. A323 (2002) 348-353.
[12] M. Guerra, C. Schmidt, J.C. McClure, L.E. Murr, A.C. Nes, Mat. Charac. 49 (2003) 95- 101.
[13] J.Q. Su, T.W. Nelson, R. Mishra, M. Mahoney, Acta Mater. 51 (2003) 713-729
[14] C.G. Rhodes, M.W. Mahoney, W.H. Bingel, Scripta Mater. 36 (1997) 69-75.
[15] G. Liu, L.E. Murr, C.S. Niou, J.C. McClure, F.R. Vega, Scripta Mater. 37 (1997) 355.
[16] L.E. Murr, G. Liu, J.C. McClur, J. Mater. Sci. Lett. 16 (1997)1801.
[17] P. Heurtier, C. Desrayaud, F. Montheillet, Mater Sci Forum 396-402 (2002) 1537.
[18] P. Bala Srinivasan, W. Dietzel, R. Zettler, J.F. Dos Santos, V. Sivan, Mater. Sci. Eng. A 392 (2005) 292-300.
[19] W.B. Lee, Y.M. Yeon, S.B. Jung, J Mater Sci Lett. 38 (2003) 4183-4191.
[20] W.B. Lee, Y.M. Yeon S.B. Jung, Scripta Mater 49 (2003) 423-428.
[21] H. Uzun, C. Dalle Donne, A. Argagnotto, T. Ghidini, C. Gambaro, Mater. Design 26 (2005) 41-46.
[22] C.M. Chen, R. Kovacevic, Int. J. Mach. Tool. Manuf. 44 (2004) 1203-1214.
[23] A.C. Somasekharan, L.E. Murr, Mater. Charact. 52 (2004) 49-64.
[24] Y. Li, E.A. Trillo, L.E. Murr, J. Mater. Sci. Lett. 19 (2000) 1047-1051.
[25] E.Cerri, P. Leo, P.P. De Marco, D. Embury, X. Wang, 'Aluminium Alloys – Their Physical and Mechanical Properties' edited by J. Hirsch, B. Skrotzki and G. Gottstein, (2008) Wiley-VCH (DE), ISBN 978-3-527-32367-8, pp. 1917-1923.
[26] A.F. Norman, I. Brough, P.B. Pragnell, Mater. Sci. Forum 331-337 (2000) 1713
[27] M.A. Sutton, B. Yang, A.P. Reynolds, J. Yan, J. Mat. Sci. Eng. A 364 (2004) 66
[28] R. Nandan, T. DebRoy, H.K.D.H. Bhadeshia, Progress in Materials Science 53 (2008) 980-1023.
[29] E. Cerri and P. Leo, Materials and Design 31 (2010) 1392–1402.
[30] C. Genevois, D. Fabrègue, A. Deschamps, W.J.Poole, Mat. Sci. Eng. A 441 (2006) 39-48.
[31] Saad A.K., Shibayanagi T., Trans. of JWRI, vol.36 (2007), no.1, 27-40.
[32] V. Dixit, R.S. Mishra, R.J. Lederich, and R. Talwar, report AFRL-ML-WP-TP-2006-468 (2006)

Abstract

Studio delle proprietà meccaniche e microstruttura di giunti FSW ultra sottili dissimili in lega di alluminio

Keywords: alluminio e leghe, precipitazione, deformazioni plastiche, saldatura, difrattometria, metallografia, microscopia elettronica, prove meccaniche

Giunti sottili di spessore 0,8mm sono stati ottenuti per Friction Stir Welding, unendo lamine di 6082T6 e 2024T3. I giunti FSW sono stati sottoposti ad una serie di prove di trazione a temperature ambiente e a temperature intermedie, nell'intevallo di 170°-230°C e velocità di deformazione comprese tra 10^{-3} e 10^{-5} s^{-1} allo scopo di valutare la deformabilità plastica dei giunti stessi. Le temperature di deformazione scelte sono tipiche temperature di invecchiamento per le due leghe in questione, per cui queste prove di trazione combinano la deformazione plastica a temperature tipiche dell'invecchiamento.
L'evoluzione microstrutturale dei giunti ultra sottili è stata studiata con microscopia ottica in luce polarizzata, microscopia elettronica in trasmissione e diffrattometria X. I giunti sottili hanno mostrato la capacità di sopportare tensioni sia a temperature ambiente che a temperature intermedie. La tensione di solito diminuiva con l'aumentare della temperatura di prova e il decrescere della velocità di deformazione. La duttilità di questi giunti è risultata in genere bassa ed indipendente dalle condizioni di prova. Poichè lo scopo di condurre test a quelle temperature era anche la valutazione della capacità di questi giunti di essere deformati in processi tecnologici come stampaggio o operazioni simili, si è evidenziato che la deformazione a temperature intermedia induce una diminuzione nella tensione di flusso e questo può essere positive, ma non risulta un livello di duttilità tale da permettere forti deformazioni di questi giunti.
Le osservazioni al TEM effettuate sui materiali base e sui giunti deformati, hanno mostrato la presenza di precipitati e costituenti microstrutturali appartenenti ai due sistemi di leghe coinvolte nel processo di FSW, in funzione del trattamento della lamiera pre-saldatura ed in funzione della esposizione alle temperature coinvolte nel processo e nella deformazione.
I campioni hanno mostrato la zona di frattura sempre in mezzo al nugget con un meccanismo di frattura duttile, sia a temperatura ambiente che a temperature superiori. Inoltre, anche se la duttilità è più o meno la stessa in campioni deformati in condizioni diverse, la distribuzione e le dimensioni dei microvuoti differisce da campione a campione, probabilmente in funzione del meccanismo dominante di nucleazione.